Nuclear Engineering and Technology 55 (2023) 1036–1044

Contents lists available at ScienceDirect

Nuclear Engineering and Technology

journal homepage: www.elsevier.com/locate/net

Original Article

Assessment of neutron-induced activation of irradiated samples in a research reactor

Ildikó Harsányi [a], András Horváth [a], Zoltán Kis [a], Katalin Gméling [a], Daria Jozwiak-Niedzwiedzka [b], Michal A. Glinicki [b], László Szentmiklósi [a, *]

[a] Centre for Energy Research, Budapest, Hungary
[b] Institute of Fundamental Technological Research, Polish Academy of Sciences, Warsaw, Poland

ARTICLE INFO

Article history:
Received 19 July 2022
Received in revised form
8 November 2022
Accepted 8 November 2022
Available online 16 November 2022

Keywords:
MCNP6
Monte Carlo simulations
FISPACT
Isotope inventory
Radioisotope production
Neutron activation analysis
Mineral aggregate
Radiation shielding concrete

ABSTRACT

The combination of MCNP6 and the FISPACT codes was used to predict inventories of radioisotopes produced by neutron exposure of a sample in a research reactor. The detailed MCNP6 model of the Budapest Research Reactor and the specific irradiation geometry of the NAA channel was established, while realistic material cards were specified based on concentrations measured by PGAA and NAA, considering the precursor elements of all significant radioisotopes. The energy- and spatial distributions of the neutron field calculated by MCNP6 were transferred to FISPACT, and the resulting activities were validated against those measured using neutron-irradiated small and bulky targets. This approach is general enough to handle different target materials, shapes, and irradiation conditions. A general agreement within 10% has been achieved. Moreover, the method can also be made applicable to predict the activation properties of the near-vessel concrete of existing nuclear installations or assist in the optimal construction of new nuclear power plant units.

1. Introduction

Research reactors are used for decades as neutron sources to produce radioisotopes for medical and industrial applications [1], to study the elemental composition of samples [2], or the radiation-induced degradation of the mechanical properties [3]. These applications developed their procedures and conventions to account for the observed reaction rates, by describing the properties of the neutron field, as well as the time-integrated fluence during irradiation. In many fields, e.g. radiation damage, or isotope production via a threshold reaction, only neutrons falling into a specific energy range are effective [4], and the others are even disadvantageous, so the use of appropriate neutron filters (e.g. cadmium, boron-carbide [5]) might be necessary.

The experimental characterization of the neutron field usually relies on the irradiation of flux monitor foils. In isotope production applications, one may use the sub-cadmium flux and the total flux as probed with a gold foil with or without a Cd cover. In k_0-neutron activation analysis (NAA) [6], the combination of Au 0.1%-Al (IRMM-530), Zr, and Fe monitor foils are used (bare triple monitor method) [7], while in the radiation damage studies [8], Al, Nb, Co, and other long-lived isotopes are applicable.

Nowadays, the non-routine irradiation requests are more abundant and increasingly well-specified (e.g. not a minimum activity, but a target activity is requested, gamma dose-rate and temperature constraints are given). Moreover, the target assemblies may contain exotic isotopes in specific geometries. For these isotopes no hands-on experience at the irradiation facility may exist, several trial-and-error test irradiations might be necessary to select the appropriate irradiation channel and optimize the conditions. Further, the predictions relying on the almost undisturbed neutron field, as determined by activation foils and the related activation equations [9], do not necessarily consider the depression of the neutron field for bulky and/or highly-absorbent target materials, nor the effect of neutron resonance shielding [10]. Therefore, a rigorous assessment of the irradiation conditions, the resulting reaction rates, neutron-induced activities [11], and dose-rate levels have become essential for such irradiation applications. This calls for a generalized computational approach.

* Corresponding author.
E-mail address: szentmiklosi.laszlo@ek-cer.hu (L. Szentmiklósi).

https://doi.org/10.1016/j.net.2022.11.004

Coherent handling of the sample activation is possible by employing full-scale Monte Carlo computer simulations of the irradiation facility, where the complex interactions between the target and the impinging particles are all considered, coupled to isotope-inventory calculations via one of the well-established FISPACT [12], CINDER [13], ACTYS [14], or ORIGEN [15] codes [16,17]. These solve the Bateman-Rubinson differential equations numerically and keep track of the time-dependent growth and decay of all relevant radionuclides at any time instances.

2. Experimental

The Budapest Research Reactor (BRR) is a tank-type research reactor with thermal power of 10 MW, moderated and cooled by light water. The reactor core is surrounded by a solid beryllium reflector. The maximum thermal flux in the core is about 2.2×10^{14} n/cm^{2}s. Unlike common reactor types, the BRR has a unique core geometry, where the 190 pieces of 19.75% enriched VVR-M2 type (LEU) fuel elements are arranged in a hexagonal pattern. In addition, the core assembly accommodates 3 safety- (SCRAM), 14 shim- and 1 fine-automatic control rods made of boron carbide and fitted with 40 vertical irradiation channels.

In this study, we focused on the characterization of the BRR's No. 17 vertical channel, where the irradiations for instrumental neutron activation analysis take place, and for which a vast amount of historical flux measurements are available. In this channel, one can stack five aluminum irradiation capsules on each other. Each of these can contain up to six hermetically sealed quartz ampoules of six or eight mm in diameter, encapsulating the individual samples to analyze, with typical masses of 125–175 mg each. The whole channel rotates around its vertical axis to compensate for any spatial inhomogeneity of the neutron flux at the actual vertical irradiation levels. In the simulations, therefore, we can reproduce this characteristic by defining six identical samples packed together, for each run and taking their average as the representative result.

The specific activities of the irradiated samples were measured using the D4 and D5 low-background gamma spectrometers of the NAA lab [18]. At first, we determined the activities of neutron flux monitor foils and powdered samples irradiated in the No. 17 channel of the reactor. After the validation of the simulation values with the measured activities for these quasi-point sources, the scope was extended to a case of bulky samples. For this purpose, a set of $18 \times 18 \times 80$ mm^3 cement mortar bars was used. Mortar bars were prepared with the water to cement ratio of 0.47 and mineral aggregates of the maximum aggregate size of 2 mm. The mineral materials were selected to cover a wide range of mineralogical compositions of rocks that determine the mechanical properties, and are useful for the production of concrete for nuclear power plant structures. The design of cement-based composites was guided by the criteria of concrete performance during long-time plant operation and the activation of concrete constituents to be considered during plant decommissioning [19]. The following rocks and minerals were included: granite, quartzite, limestone, trachybasalt, opal, and flint. Powder specimens were manufactured by grinding virgin rock aggregates and cement mortar bars, down to the size <45 μm. The mortar bars, as well as their grounded forms, were finally irradiated in the Budapest Research Reactor. All ingredients were previously analyzed by NAA [18] and PGAA [20] for their elemental mass fractions and this information was used to set up accurate material cards for the MCNP and FISPACT codes. The combined PGAA and NAA measurements provided the concentrations of several low-Z elements (H, B, C, O, Cl), the significant major matrix components (Na, Al, Mg, Si, K, Ca, Fe), as well as many trace components (e.g. Sm, Gd, Co, Cs, Eu Ba, La). By reporting more than 20 trace elements overall, as tabulated in the Electronic Supplementary Information, this composition analysis procedure is more comprehensive than the usual XRF data. This combination of experimentally-obtained concentrations and calculations for the prediction of neutron-induced activation was named NEAAA (*neutron-based elemental composition analysis and activity assessment*).

3. Methodology

3.1. Monte Carlo simulations of the irradiation

Monte Carlo simulations were published for standardized and widespread research reactor types, such as the TRIGA [21,22] and SLOWPOKE [23–25], mostly for reactivity and thermohydraulic calculations, or for decommissioning [26–29]. The use of this technique for irradiation planning, sample activation [30,31], or sample clearance studies is still uncommon.

To establish such a tool for the unique core assembly of the Budapest Research Reactor, an MCNP6.2 [32] simulation model of the core was constructed, where the neutron-field properties, such as the integrated intensity, spatial- and energy distributions, could be calculated for any irradiation positions. The geometry of the MCNP model, and that of the irradiation channel No 17, is presented in Fig. 1.

The neutron flux specified by MCNP in the so-called F4 track length estimates per volume tally(Φ_{F4}) are normalized per source neutron. To get to the real flux intensity, this must be scaled up using Eq. (1):

$$\Phi = \frac{P \bullet \bar{\nu}}{1.622 \times 10^{-13} \bullet w_f} \frac{1}{k_{eff}} \Phi_{F4} = 7.646 \bullet 10^{17} \Phi_{F4} \quad (1)$$

where P is the reactor thermal power, $\bar{\nu}$ is the average number of neutrons produced per fission, w_f is the energy released per fission, k_{eff} the calculated reactor multiplication factor, and Φ_{F4} is the flux normalized per source neutron [cm^{-2}] from the MCNP output [33].

The case of bulky samples was assessed also by using F4 tallies, where FM cards were set up for the radiative neutron capture reaction (ID 102 from the ENDF library) of each relevant isotope, printing out the volumetric average of the neutron capture rate per isotope of interest in the entire volume of the sample. This simulation was repeated with the identical geometry, but with a target material density reduced by a factor of 1000, representing an infinitely diluted matrix. The ratio of the capture reaction rates with and without dilution, and normalized with the dilution factor, provided the neutron self-shielding correction factor of the voluminous sample. The subsequent isotope inventory calculations are multiplied by this factor to arrive at a well-justified activation estimation for the real sample geometry. For visualization of the flux depression, in some cases, we also used 3D mesh tallies, which provide the spatial distribution of all these quantities.

3.2. Monte Carlo simulations of the activity measurement

The experimental activities of the irradiated samples were measured using well-calibrated HPGe detectors placed inside a low-level iron counting chamber [18]. To consider the gamma self-absorption and efficiency variation of the bulky samples for the activity measurement, the MCNP model of the gamma spectrometer was also established. We used SuperMC [34] to machine-convert the CAD geometries of the iron counting chamber and the detector (except for the dimensions of the crystal) to MCNP format. Subsequently, the details of the Ge crystal were set up based on the fine-tuned values of the factory-specified dimensions.

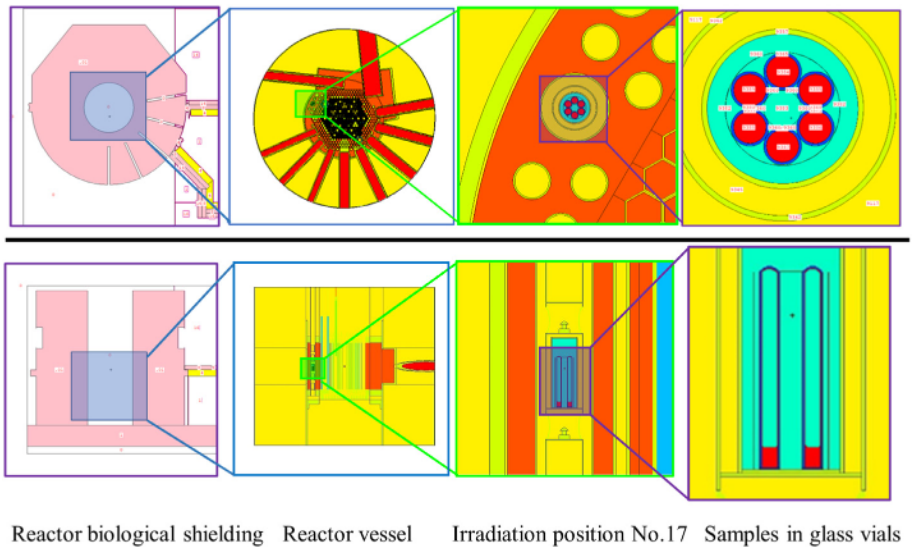

Fig. 1. Horizontal and vertical cuts of the MCNP reactor model, gradually zooming in to the details of the irradiation position No 17. Materials are color-coded: pink (concrete biological shielding), yellow (cooling water), red (iron structure), orange (beryllium reflector), light-blue (air), dark-blue (silicon sample vial), and purple-red (NAA powder sample).

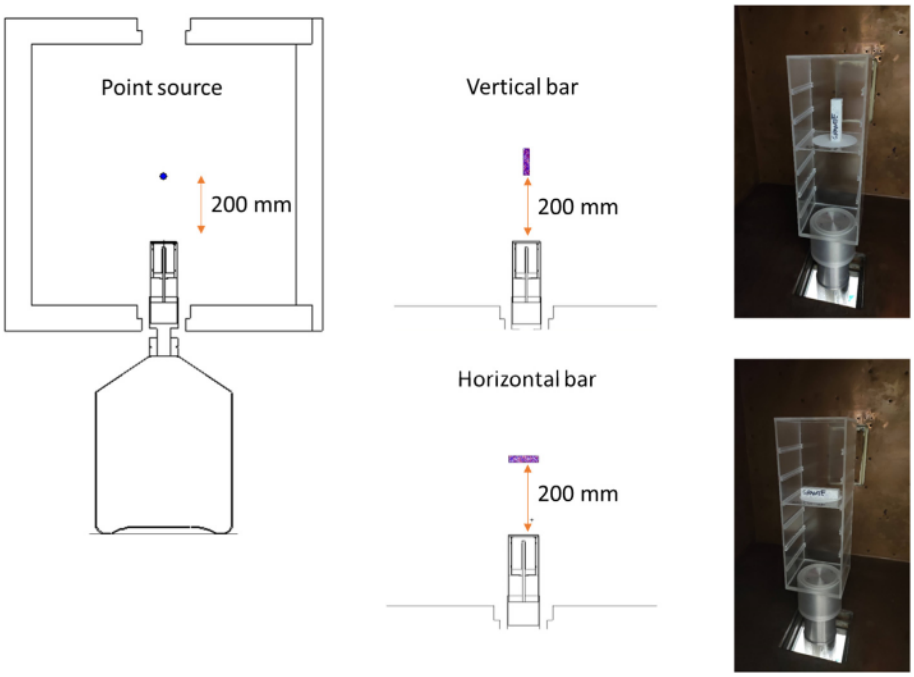

Fig. 2. The MCNP model of the gamma spectrometer to establish the efficiency transfer function of bulky samples.

With MCNP, the ratio of the counts in the real geometry and the corresponding point-source geometry was calculated, and this efficiency transfer function was used to scale the experimental efficiency curve of the spectrometer (measured using certified sealed point sources). These activities, being corrected for the geometric effect and the gamma self-absorption, were used to benchmark FISPACT.

3.3. Isotope inventory calculations by FISPACT

Using the neutron field parameters and the composition of the target, a radioisotope inventory for any time instance can be obtained by using either the MCNP's built-in CINDER routines or in our case, by the FISPACT code. The best coupling was achieved between MCNP and FISPACT when the F4 tally data were tabulated according to the CCFE-709 group energy structure [35], one of the native energy-bin sets of FISPACT, ranging from 10^{-5} eV–10^{9} eV. This way, the inaccuracy related to internal energy-spectrum rebinning could be avoided, which, for instance, created unrealistic discontinuities when feeding in the neutron spectrum according to the UKAEA-1102 tabulation. We used the FISPACT's TENDL-2017 nuclear data library for our calculations.

These FISPACT activity calculations not only account for the major contributors to gamma dose rate but also for the decays to the ground state, that are without gamma emission, or decays emitting very low-energy gamma radiation that falls below the low-level discriminator of the gamma spectrometer. These are invisible to our NAA experiments but still can contribute to the total activity of the samples.

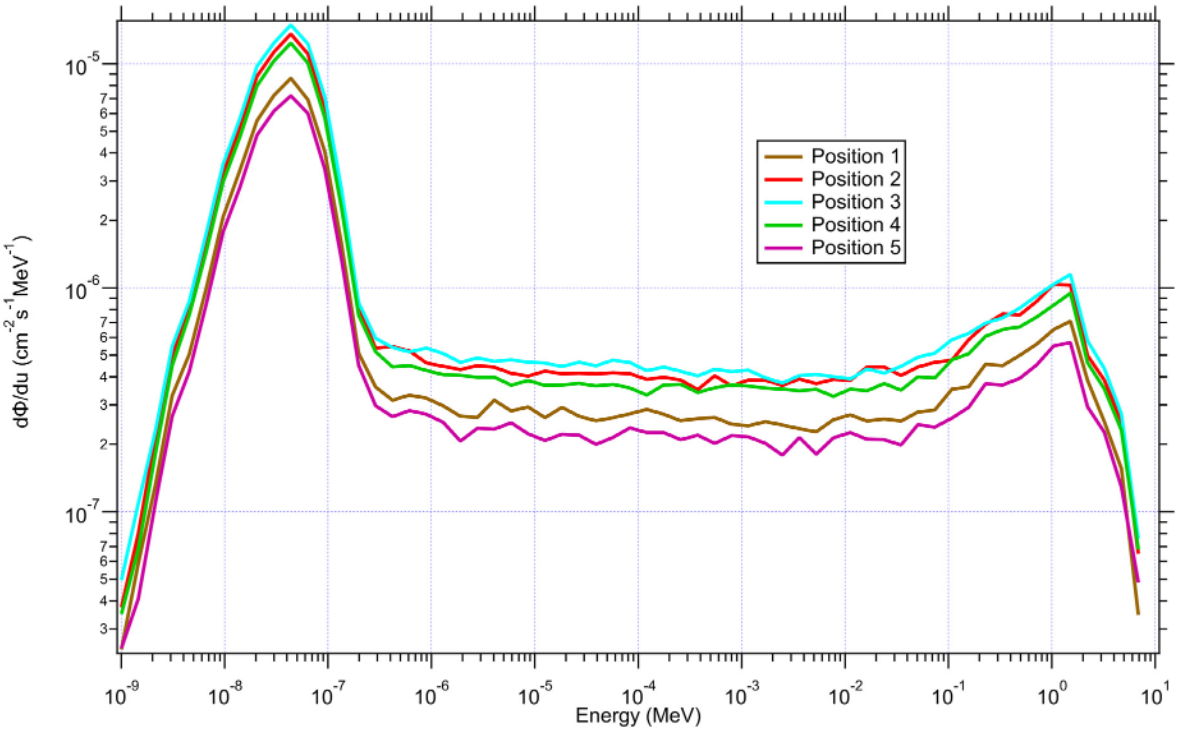

Fig. 3a. The energy distribution of the neutron flux for the five vertical positions of the No. 17 channel.

4. Results and discussion

4.1. Activation of flux monitors

After applying the scaling factor of Eq. (1), the MCNP-calculated energy distribution of the neutron fluxes at the five vertical positions of the No. 17 channel is depicted in Fig. 3a, while the vertical flux profile along the long axis of the channel is shown in Fig. 3b. We can conclude that the energy distributions are similar and differ only in their amplitudes. The absolute flux has its maximum near the center plane of the core and shows a parabolic profile. Note that the presence of the NAA samples and the sample containers have a considerable impact on the magnitude of the neutron flux compared to the undisturbed neutron field.

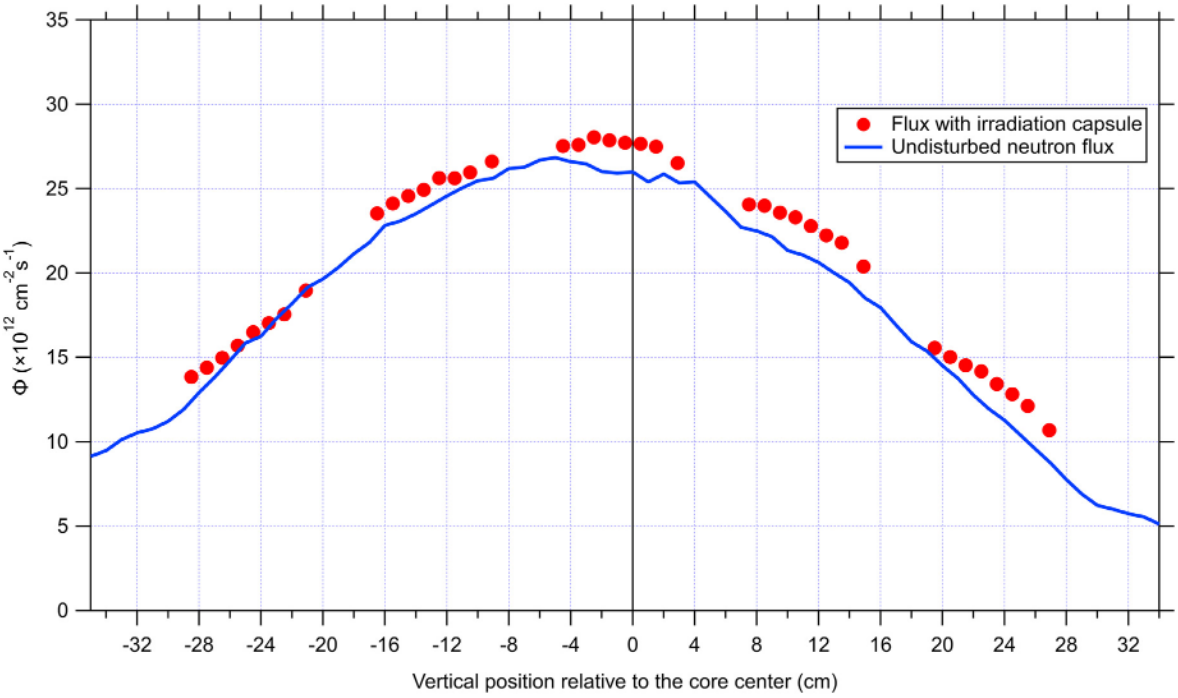

Fig. 3b. The simulated vertical neutron intensity profile in the five positions (1–5 from left to right) of the No. 17 channel.

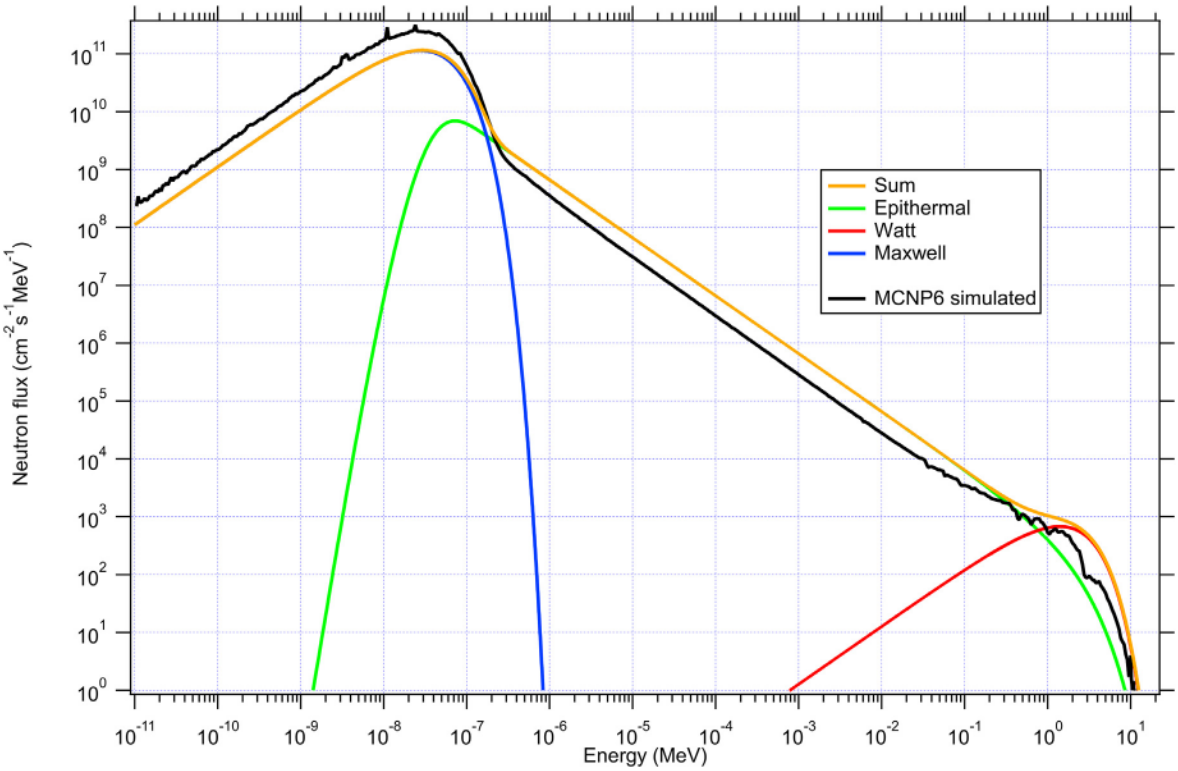

Fig. 4a. the measured (orange) vs. calculated (black) flux distributions in Pos. 2 of the No. 17 channel.

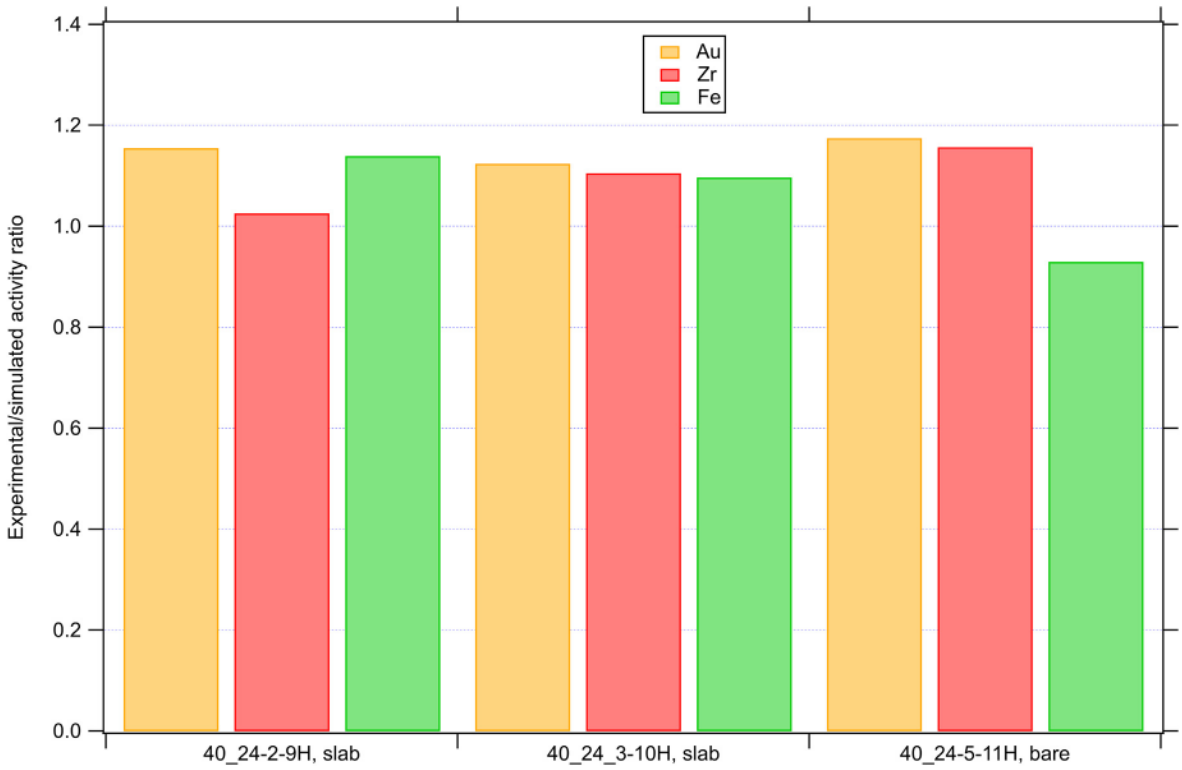

Fig. 4b. the measured over calculated activities of Au 0.1%-Al (IRMM-530), zirconium, and iron foils irradiated in Pos. 2 of the No. 17 channel.

The parabolic neutron intensity profile has no negative consequence on routine NAA since the point-like sample and the flux monitor foils are placed close to each other and interact with the same local neutron field. This is, however, not the case for bulky sample irradiations, where the tiny flux monitor and the bulky sample may sense different neutron intensities, making the upscaling of small-sample results inaccurate without a correction. This is in line with the conclusions of Overwater and Hoogenboom [36].

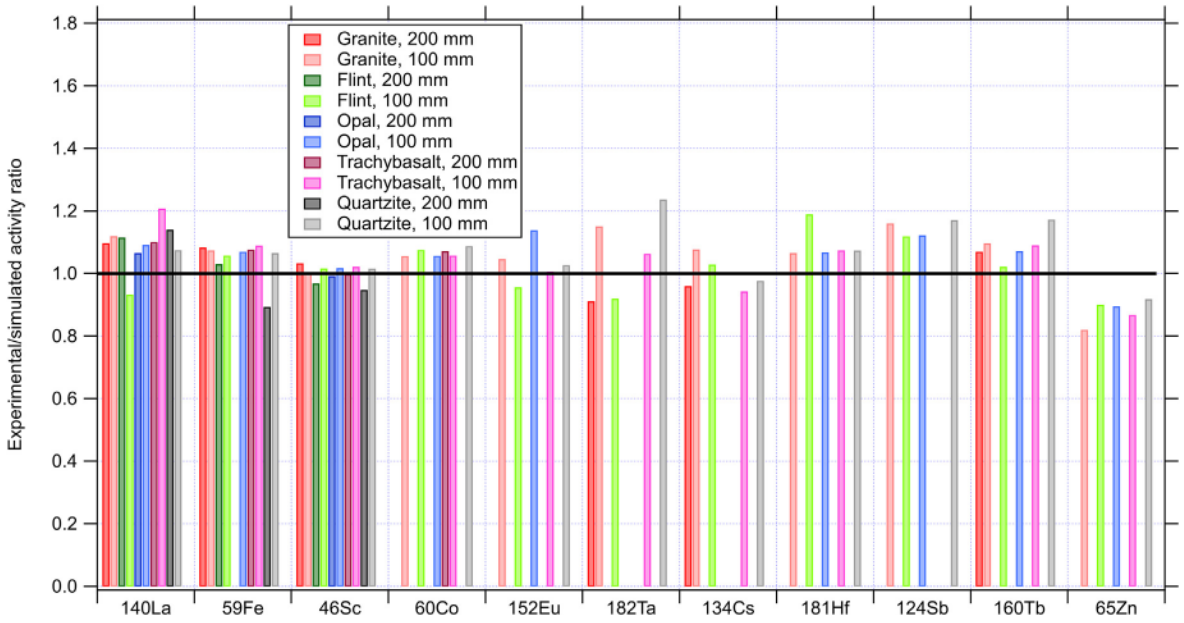

Fig. 5. The ratios of the measured and predicted activities for the ground mortars loaded with various additives, in a point-source geometry. The first gamma counting has been done at a 200 mm sample-to-detector distance, while the second at 100 mm.

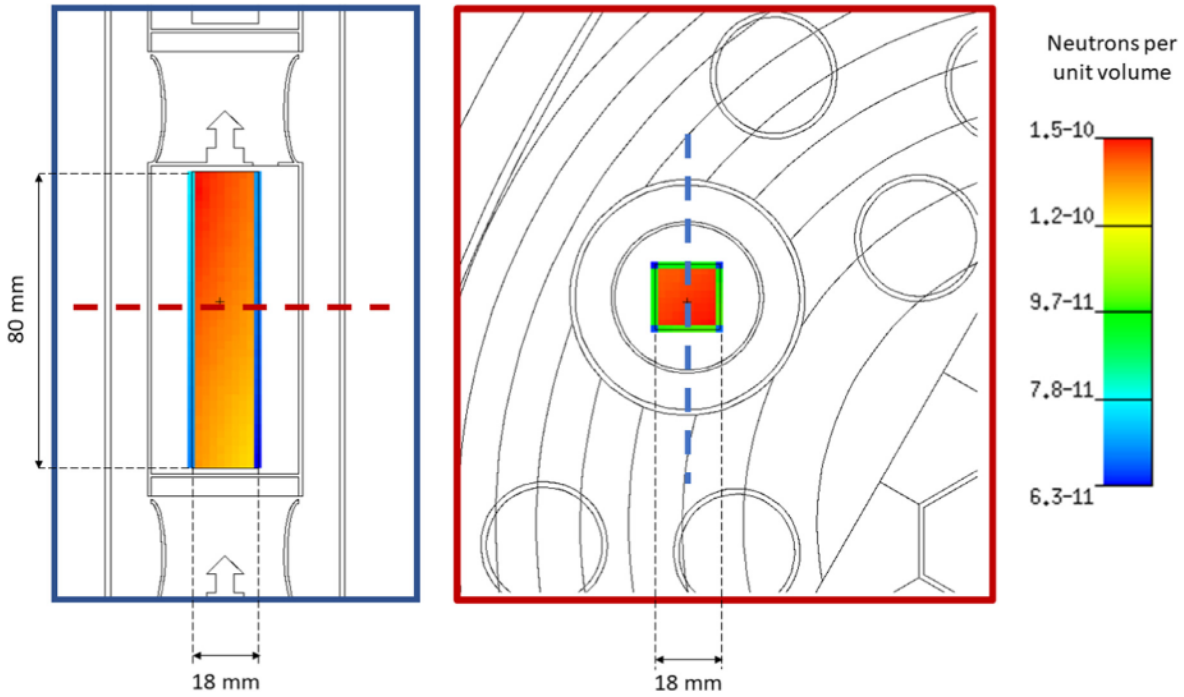

Fig. 6. The neutron flux intensity within the granite-loaded mortar test sample from MCNP simulation.

The experimental neutron flux distribution, established according to the k_0-neutron activation analysis (NAA) convention, showed good similarity to the MCNP-simulated curve, as visualized in Fig. 4a. After transferring the simulated flux distribution to FISPACT and calculating the activities of the monitor foils for the respective experimental cooling times, a decent agreement was observed with the experimental activation data, as shown in Fig. 4b.

4.2. Activation of powdered materials

The activation properties of ground mortar samples were also successfully reproduced by the FISPACT. Here the emphasis was laid on the long-lived radioisotope contents, as they influence most of the post-irradiation sample clearance issues as well as the decommissioning costs of a nuclear facility. As shown in Fig. 5, we were able to reproduce the measured activation within about 10%, while the uncertainty margin of the experimental vs simulated

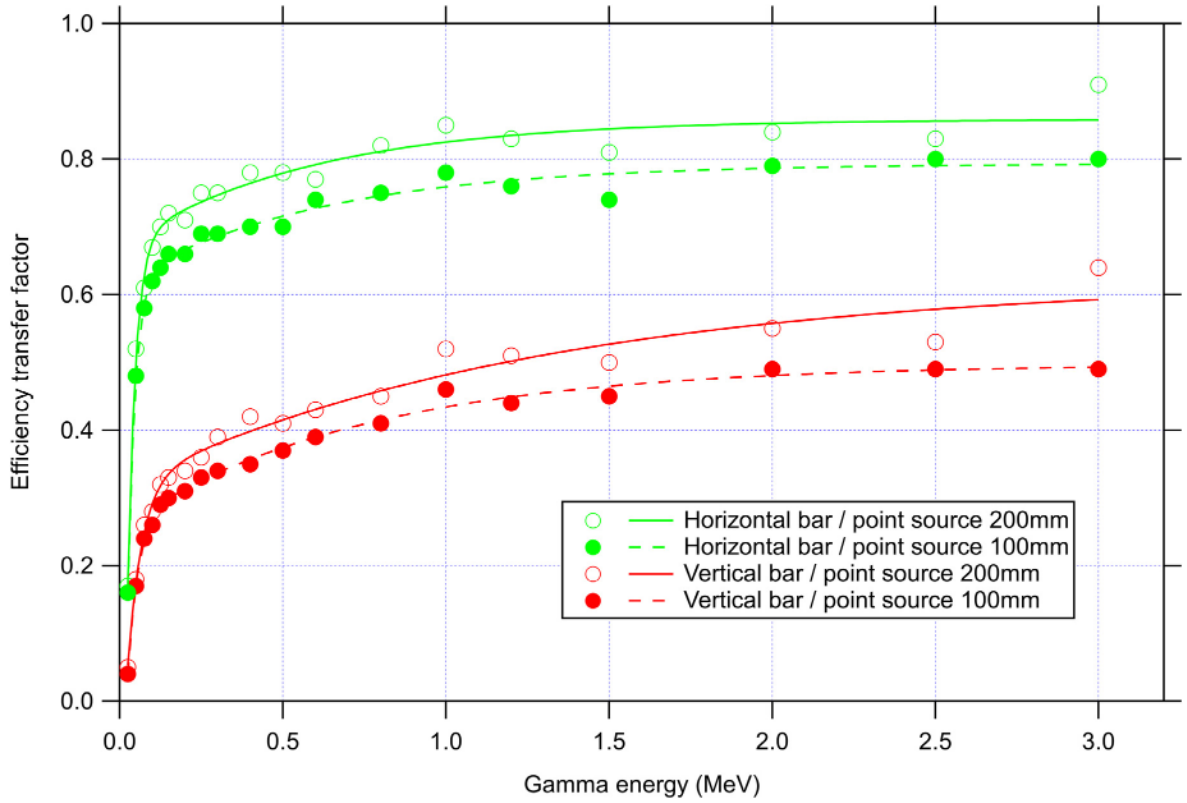

Fig. 7. The efficiency-transfer factors between horizontally and vertically placed bulky samples and corresponding point sources.

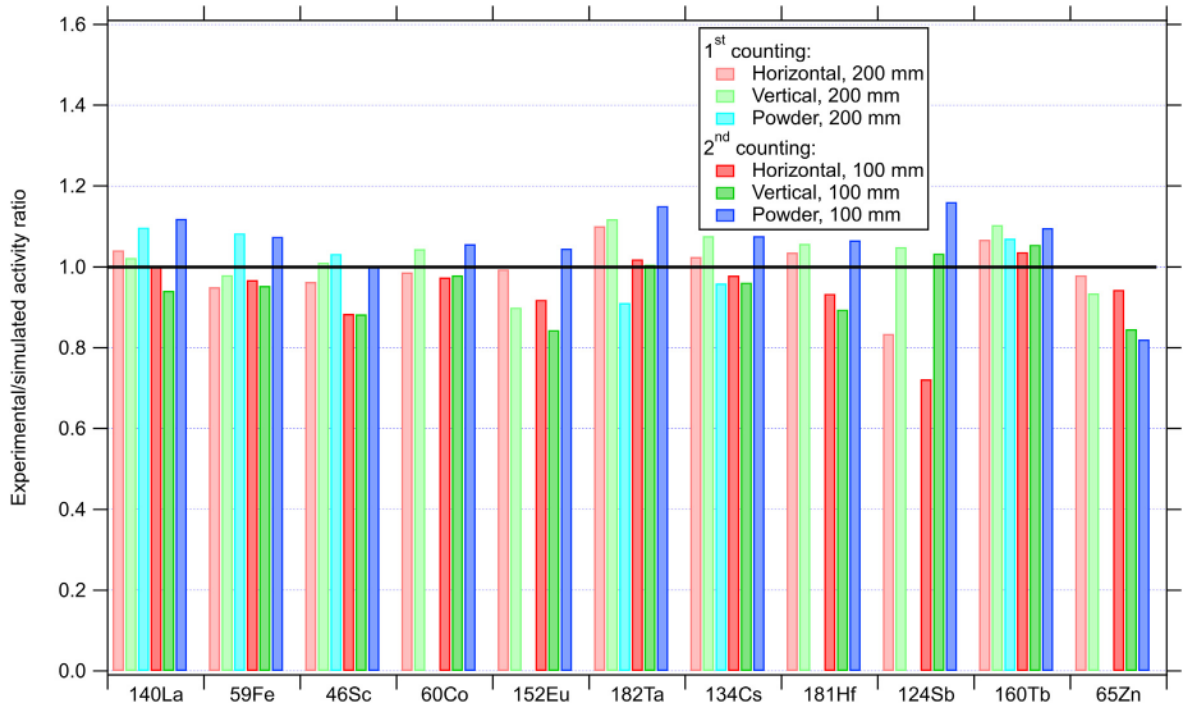

Fig. 8. The experimental activity divided by the simulated activity for the horizontally and vertically placed granite-loaded mortar bars, as well as the corresponding point-like ground sample. The first gamma-measurement took place at 200 mm, 100–150 h after irradiation, while the second run at 100 mm, 250–400 h after irradiation. Note that not every radionuclide was detectable in all measurements.

ratios was about 5%. Missing bars mean that the radioisotope was not detected experimentally in the given sample so the ratio could not be calculated.

4.3. Activation of bulky mortar samples

In the case of the bar samples, neither the neutron self-shielding nor the gamma self-absorption was found to be negligible. The former effect is visualized in Fig. 6, where a vertical and a horizontal cut of the 3D simulation mesh are shown, sampling the number of neutrons per unit volume. There is a gradient of the neutron intensity of about 20% that is fully consistent with the results of Fig. 3b.

The latter effect, i.e. the combination of gamma self-absorption and the change in the solid angle during gamma-spectrometry measurements was also simulated, using the detector geometry shown in Fig. 2. The efficiency-transfer functions [37] relative to a point source were obtained for the horizontal and vertical placements of the bars, for both 100 mm and 200 mm sample-to-detector distances (Fig. 7). When we applied these correction curves, a very good agreement was achieved between the measured and simulated data for most of the relevant radionuclides, not only for the powdered case but also for horizontal and vertical solid bar geometries. This is evidenced in Fig. 8.

5. Conclusions and outlook

We worked out the NEAAA method, i.e. the combination of i) experimental composition measurement by PGAA and NAA, ii) MCNP-based irradiation calculations, and iii) FISPACT-based radioisotope inventory calculations, to predict the activation of targets placed into a vertical channel of the Budapest Research Reactor. This approach is general enough to handle different target materials, shapes, and irradiation conditions. The calculations were validated with irradiations at the No 17 vertical channel of our reactor at 10 MW power. Flux monitor foils, multi-component powdered NAA samples, and bulky mortar bars were tested, showing increasing complexity, and a decent agreement was achieved in all cases. The ratios of experimental and simulated activities agreed typically within 10%, while the uncertainty margin was about 5%–30%.

Within the framework of the V4-Korea RADCON project, a systematic study was conducted, sampling all significant domestic gravel and sand mines of Hungary [38], as well as raw material suppliers of cement and other additives. Based on this comprehensive simulation methodology, raw material dataset, and the mixing design of the concrete, our goal is to predict the activation properties of the near-vessel concrete of existing nuclear installations by computer simulations as well as apply it to the optimal construction of new nuclear power plant units.

Author contributions

H.I: Software, Validation (FISPACT), Investigation, Data Curation, Formal analysis (PGAA); A.H, Z.K: Methodology, Software (MCNP); K.G. Investigation, Data Curation, Formal analysis (NAA), D.J.N., M.A.G: Resources (Preparation of mortar bars), Funding acquisition; L.Sz: Conceptualization, Methodology, Validation, Resources, Writing - Original Draft, Visualization, Supervision, Project administration, Funding acquisition.

Declaration of competing interest

The authors declare that they have no known competing financial interests or personal relationships that could have appeared to influence the work reported in this paper.

Acknowledgment

This work was part of the V4-Korea RADCON Project (No. 127102) and received support from the National Research, Development and Innovation Fund of Hungary, financed under the NN_17 funding scheme. We thank the financial contribution of the TOURR project (Euratom research and training programme 2019–2020, grant agreement No. 945269). We also acknowledge the valuable collaboration with Péter Juhász, Dávid Hajdú and Viktória Sugár, Gábor Patriskov, Tamás Bozsó, as well as with the ÉMI Non-profit Llc.

Appendix A. Supplementary data

Supplementary data to this article can be found online at https://doi.org/10.1016/j.net.2022.11.004.

References

[1] International Atomic Energy Agency, Applications of Research Reactors, INTERNATIONAL ATOMIC ENERGY AGENCY, Vienna, 2014. https://www.iaea.org/publications/10491/applications-of-research-reactors.
[2] S.J. Parry, Activation Analysis | Neutron Activation, Encycl. Anal. Sci., 2019, pp. 15–24, https://doi.org/10.1016/B978-0-12-409547-2.14532-9.
[3] International Atomic Energy Agency, Research Reactor Application for Materials under High Neutron Fluence, INTERNATIONAL ATOMIC ENERGY AGENCY, Vienna, 2011. https://www.iaea.org/publications/8452/research-reactor-application-for-materials-under-high-neutron-fluence.
[4] A.Y. Konobeyev, U. Fischer, S.P. Simakov, Atomic displacement cross-sections for neutron irradiation of materials from Be to Bi calculated using the arc-dpa model, Nucl. Eng. Technol. 51 (2019) 170–175, https://doi.org/10.1016/j.net.2018.09.001.
[5] R. Szőke, I. Sziklai-László, Epiboron NAA: an option to analyze unfavorable matrices, J. Radioanal. Nucl. Chem. 275 (2008) 89–95, https://doi.org/10.1007/s10967-007-6977-6.
[6] F. De Corte, The k_0-Standardization Method, Rijksuniversiteit Gent, Gent, 1987.
[7] L. Hamidatou, H. Benkharfia, Experimental and MCNP calculations of neutron flux parameters in irradiation channel at Es-Salam reactor, J. Radioanal. Nucl. Chem. 287 (2011) 971–975, https://doi.org/10.1007/s10967-010-0922-9.
[8] D. Chiesa, M. Carta, V. Fabrizio, L. Falconi, A. Grossi, M. Nastasi, M. Palomba, S. Pozzi, E. Previtali, P.G. Rancoita, B. Ranghetti, M. Tacconi, Characterization of TRIGA RC-1 neutron irradiation facilities for radiation damage testing, Eur. Phys. J. Plus. 135 (2020) 349, https://doi.org/10.1140/epjp/s13360-020-00334-7.
[9] V.K. Basenko, A.N. Berlizov, I.A. Malyuk, V. V Tryshyn, NAAPRO: a code for predicting results and performance of neutron activation analysis, J. Radioanal. Nucl. Chem. 263 (2005) 675–681, https://doi.org/10.1007/s10967-005-0642-8.
[10] J. Romero–Barrientos, F. Molina, P. Aguilera, H.F. Arellano, Calculation of self–shielding factor for neutron activation experiments using GEANT4 and MCNP, AIP Conf. Proc. 1753 (2016), 080018, https://doi.org/10.1063/1.4955388.
[11] M. Blaauw, D. Ridikas, S. Baytelesov, P.S.B. Salas, Y. Chakrova, C. Eun-Ha, R. Dahalan, A.H. Fortunato, R. Jacimovic, A. Kling, L. Muñoz, N.M.A. Mohamed, D. Párkányi, T. Singh, Van Dong Duong, Estimation of 99Mo production rates from natural molybdenum in research reactors, J. Radioanal. Nucl. Chem. 311 (2017) 409–418, https://doi.org/10.1007/s10967-016-5036-6.
[12] M. Fleming, T. Stainer, M. Gilbert, The FISPACT-II User Manual, UK Atomic Energy Authority, Culcham Science Centre, Oxfordshire, 2018.
[13] T.R. England, CINDER – A One-Point Depletion and Fission Product Program WAPD-TM-384, 1962.
[14] S.C. Tadepalli, P. Kanth, G. Indauliya, I. Saikia, S.P. Deshpande, P.V. Subhash, Development and validation of ACTYS, an activation analysis code, Ann. Nucl. Energy 107 (2017) 71–81, https://doi.org/10.1016/j.anucene.2017.04.016.
[15] C. V Parks, Overview of ORIGEN2 and ORIGEN-S: Capabilities and Limitations, 1992. United States, http://inis.iaea.org/search/search.aspx?orig_q=RN:23037442.
[16] D. Hajdú, E. Dian, K. Gméling, E. Klinkby, C.P. Cooper-Jensen, J. Osán, P. Zagyvai, Experimental study of concrete activation compared to MCNP simulations for safety of neutron sources, Appl. Radiat. Isot. 171 (2021), 109644, https://doi.org/10.1016/j.apradiso.2021.109644.
[17] D. Hajdú, E. Dian, E. Klinkby, C.P. Cooper-Jensen, J. Osán, P. Zagyvai, Neutron activation properties of PE-B4C-concrete assessed by measurements and simulations, J. Neutron Res. 21 (2020) 87–94, https://doi.org/10.3233/JNR-190126.
[18] L. Szentmiklósi, D. Párkányi, I. Sziklai-László, Upgrade of the Budapest neutron activation analysis laboratory, J. Radioanal. Nucl. Chem. 309 (2016), https://doi.org/10.1007/s10967-016-4776-7.

[19] D. Jóźwiak-Niedźwiedzka, K. Gméling, A. Antolik, K. Dziedzic, M.A. Glinicki, Assessment of long lived isotopes in Alkali-Silica resistant concrete designed for nuclear installations, Materials 14 (2021) 4595, https://doi.org/10.3390/ma14164595.
[20] L. Szentmiklosi, T. Belgya, Z. Revay, Z. Kis, Upgrade of the prompt gamma activation analysis and the neutron-induced prompt gamma spectroscopy facilities at the Budapest research reactor, J. Radioanal. Nucl. Chem. 286 (2010) 501–505.
[21] A.D. Loya, S.V. Escamilla, A.M.G. Torres, E.D.V. Gallegos, Verification of a Triga Mark III MCNP model for neutron flux calculations, Int. J. Nucl. Energy Sci. Technol. 10 (2016) 146, https://doi.org/10.1504/IJNEST.2016.077480.
[22] A. Borio di Tigliole, A. Cammi, D. Chiesa, M. Clemenza, S. Manera, M. Nastasi, L. Pattavina, R. Ponciroli, S. Pozzi, M. Prata, E. Previtali, A. Salvini, M. Sisti, TRIGA reactor absolute neutron flux measurement using activated isotopes, Prog. Nucl. Energy 70 (2014) 249–255, https://doi.org/10.1016/j.pnucene.2013.10.001.
[23] F. Puig, H. Dennis, SLOWPOKE-2 alternative core loading configurations analysis for highly improved reactor performance, Ann. Nucl. Energy 128 (2019) 216–230, https://doi.org/10.1016/j.anucene.2018.12.016.
[24] J.C. Rook, K.P. Weber, E.C. Corcoran, Advanced MCNP simulation of the neutron and photon flux and absorbed dose rates for the SLOWPOKE-2 nuclear reactor at the royal Military College of Canada, Nucl. Technol. 206 (2020) 1861–1874, https://doi.org/10.1080/00295450.2020.1720557.
[25] T.S. Nguyen, G.B. Wilkin, J.E. Atfield, Monte Carlo calculations applied to SLOWPOKE full-reactor analysis, AECL Nucl. Rev. 1 (2012) 43–46, https://doi.org/10.12943/anr.2012.00017.
[26] A. Septilarso, D. Kawasaki, S. Yanagihara, Radioactive waste inventory estimation of a research reactor for decommissioning scenario development, J. Nucl. Sci. Technol. 57 (2020) 253–262, https://doi.org/10.1080/00223131.2019.1667923.
[27] A. Räty, P. Kotiluoto, FiR 1 TRIGA activity inventories for decommissioning planning, Nucl. Technol. 194 (2016) 28–38, https://doi.org/10.13182/NT15-86.
[28] B. Volmert, M. Pantelias, R.K. Mutnuru, E. Neukaeter, B. Bitterli, Validation of MCNP NPP activation simulations for decommissioning studies by analysis of NPP neutron activation foil measurement Campaigns, EPJ Web Conf. 106 (2016), 05010, https://doi.org/10.1051/epjconf/201610605010.
[29] B. Babcsány, S. Czifrus, S. Fehér, Methodology and conclusions of activation calculations of WWER-440 type nuclear power plants, Nucl. Eng. Des. 284 (2015) 228–237, https://doi.org/10.1016/j.nucengdes.2014.11.032.
[30] S. Kim, M.H. Kim, A study on MCNPX-CINDER90 system for activation analysis, in: Trans. Korean Nucl. Soc. Autumn Meet, 2014, pp. 5–8. Pyeongchang, Korea.
[31] V. Radulović, R. Jaćimović, A. Pungerčič, I. Vavtar, L. Snoj, A. Trkov, Characterization of the neutron spectra in three irradiation channels of the JSI TRIGA reactor using the GRUPINT spectrum adjustment code, Nucl. Data Sheets 167 (2020) 61–75, https://doi.org/10.1016/j.nds.2020.07.003.
[32] T. Goorley, M. James, T. Booth, F. Brown, J. Bull, L.J. Cox, J. Durkee, J. Elson, M. Fensin, R.A. Forster, J. Hendricks, H.G. Hughes, R. Johns, B. Kiedrowski, R. Martz, S. Mashnik, G. McKinney, D. Pelowitz, R. Prael, J. Sweezy, L. Waters, T. Wilcox, T. Zukaitis, Features of MCNP6, Ann. Nucl. Energy 87 (2016) 772–783, https://doi.org/10.1016/J.ANUCENE.2015.02.020.
[33] G. Žerovnik, M. Podvratnik, L. Snoj, On normalization of fluxes and reaction rates in MCNP criticality calculations, Ann. Nucl. Energy 63 (2014) 126–128, https://doi.org/10.1016/j.anucene.2013.07.045.
[34] Y. Wu, J. Song, H. Zheng, G. Sun, L. Hao, P. Long, L. Hu, CAD-based Monte Carlo program for integrated simulation of nuclear system SuperMC, Ann. Nucl. Energy 82 (2015) 161–168, https://doi.org/10.1016/J.ANUCENE.2014.08.058.
[35] UKAEA, CCFE-709 group structure, (n.d.). https://fispact.ukaea.uk/wiki/CCFE-709_group_structure.
[36] R.M.W. Overwater, J.E. Hoogenboom, Accounting for the thermal neutron flux depression in voluminous samples for instrumental neutron activation analysis, Nucl. Sci. Eng. 117 (1994) 141–157, https://doi.org/10.13182/NSE94-A28530.
[37] T. Vidmar, B. Vodenik, M. Nečemer, Efficiency transfer between extended sources, Appl. Radiat. Isot. 68 (2010) 2352–2354, https://doi.org/10.1016/j.apradiso.2010.05.010.
[38] V. Szilágyi, K. Gméling, S. Józsa, I. Harsányi, L. Szentmiklósi, Oligomictic alluvial aggregates: petro-mineralogical and geochemical evaluation of sandy gravel formations on the middle course of the Danube (Hungary), Bull. Eng. Geol. Environ. 80 (2021) 5957–5977, https://doi.org/10.1007/s10064-021-02271-w.